First observation of a new zonal-flow cycle state in the H-mode transport barrier of the experimental advanced superconducting Tokamak

G. S. Xu,[1,a)] H. Q. Wang,[1] B. N. Wan,[1] H. Y. Guo,[1] V. Naulin,[2] P. H. Diamond,[3] G. R. Tynan,[3] M. Xu,[3] N. Yan,[1,2] W. Zhang,[1] J. F. Chang,[1] L. Wang,[1] R. Chen,[1] S. C. Liu,[1] S. Y. Ding,[1] L. M. Shao,[1] H. Xiong,[1] and H. L. Zhao[4]
[1]*Institute of Plasma Physics, Chinese Academy of Sciences, Hefei 230031, China*
[2]*Association Euratom-Risø DTU, DK-4000 Roskilde, Denmark*
[3]*University of California, San Diego, 9500 Gilman Drive, La Jolla, California 92093, USA*
[4]*Department of Modern Physics, University of Science and Technology of China, Hefei 230026, China*

(Received 27 July 2012; accepted 20 November 2012; published online 5 December 2012)

A new turbulence-flow cycle state has been discovered after the formation of a transport barrier in the H-mode plasma edge during a quiescent phase on the EAST superconducting tokamak. Zonal-flow modulation of high-frequency-broadband (0.05–1 MHz) turbulence was observed in the steep-gradient region leading to intermittent transport events across the edge transport barrier. Good confinement ($H_{98y,2} \sim 1$) has been achieved in this state, even with input heating power near the L-H transition threshold. A novel model based on predator-prey interaction between turbulence and zonal flows reproduced this state well. © *2012 American Institute of Physics*.
[http://dx.doi.org/10.1063/1.4769852]

I. INTRODUCTION

Over the last decade, it has been progressively recognized that spontaneously generated zonal flows (ZFs) may play an important role for turbulence or transport barrier self-regulation in magnetically confined plasmas[1] and planetary atmospheres.[2] Predator-prey cycle states are ubiquitous in ecological and economic systems in which two species or industrial sectors interact, leading to periodic behavior in the evolution of their populations. In the region of a strong transport barrier, such as in the edge region of toroidal fusion plasmas when a higher confinement regime—so-called "H mode"—has been achieved, turbulence is usually thought to be suppressed by a strong shear in the plasma flows. However, instabilities and turbulence can still arise due to a strong drive by the steep pressure gradients developed there.[3] The free energy stored in the pressure gradient is then released and partially transferred into the turbulence—the prey. ZFs—the predator, fed by the turbulence through the action of the Reynolds stress,[4] will thrive since there are plenty of prey but, ultimately, outstrip their energy supply and decline. As the ZFs are low, the turbulence will increase again. In this way, the dynamics continue in a cycle of growth and decline. This predator-prey cycle state has been observed recently in several experiments[5–10] prior to the formation of a transport barrier in the edge region of toroidally magnetized plasmas as input heating power close to the L-H transition (transition from low- to high-confinement mode) power threshold. Their observations are qualitatively consistent with a new predator-prey model of the L-H transition.[11,12] However, existence of this cycle state after the transition has not been reported previously. In this paper, we report the discovery of this turbulence-flow cycle state and the resultant intermittent transport events across the strong barrier region of the H-mode plasmas during a quiescent H-phase (without any MHD activities at the plasma edge such as edge localized modes or coherent modes). The turbulence appeared in the edge barrier region is of high frequency and broadband (0.05–1 MHz) in contrast to the low-frequency (<0.2 MHz) turbulence prevailing before the transition into the H mode. These new findings may shed some light on the physics mechanism behind the self-organization dynamics of strong transport barriers in plasmas and stratified fluids.

II. EXPERIMENTAL RESULTS

The new ZF cycle state was first discovered in the 2010 H-mode campaign of the EAST superconducting tokamak ($R_0 \sim 1.9$ m, $a \sim 0.45$ m),[13] characterized by quasi-periodic oscillations on the divertor Dα signals with amplitude smaller than that of Type-III edge localized modes (ELMs) by more than one order of magnitude, as shown in Fig. 1(b) and the zoom-in plot in Fig. 1(c), where typical Type-III ELMs appear over 3.59–3.66 s. The H mode was achieved using lower hybrid current drive (LHCD) with available total heating power limited to about 1 MW, just above the L-H transition power threshold. The cycle state frequently appears shortly after the L-H transitions as shown in Fig. 1, but sometimes it also appears in the inter-ELM phase. The oscillations appear to originate from the plasma edge steep-gradient region, usually referred to as the "pedestal." The frequency of the oscillations ranges from 0.3 to 3 kHz centered near 1 kHz, and the amplitude generally decreases with increasing frequency. The frequency or amplitude does not show strong dependence on the input heating power, q_{95} or any configuration parameters.

In order to study the dynamics of the cycle state, two reciprocating Langmuir probes located at the outer midplane, toroidally separated by 89°, one in port A and the other in port E,[14] were used to provide direct measurements of radial electric field (E_r), turbulent Reynolds stress, and long-range

a)Author to whom correspondence should be addressed. Electronic mail: gsxu@ipp.ac.cn.

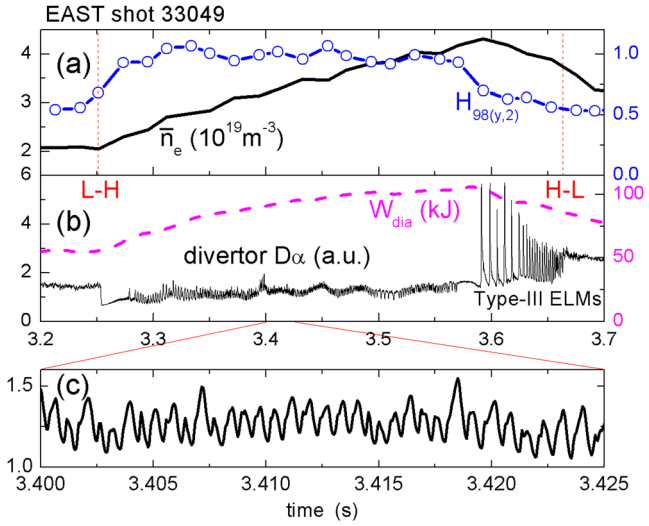

FIG. 1. (a) Central-chord-average density and $H_{98(y,2)}$, (b) Dα emission near the inner target of the lower divertor and the plasma diamagnetic energy, (c) zoom of the Dα signal.

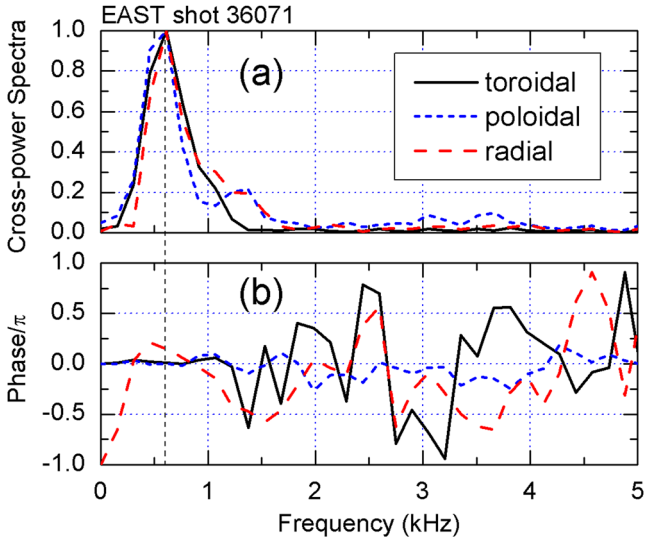

FIG. 2. Spectra of (a) cross power, (b) cross phase between floating potentials inside the separatrix at two locations toroidally separated by 89° (black solid curve), poloidally separated by 8 mm (blue dotted curve), and radially separated by 8 mm (red dashed curve), respectively. The spectrum peak at ~0.6 kHz is associated with the oscillations on the divertor Dα signals.

correlation between potential fluctuations[15] at the plasma edge with a 5 MHz sampling rate. The low heating power allows direct probing of turbulence and ZFs inside the separatrix in the H-mode plasmas using fast-moving graphite probes. A specially designed probe array was used to measure floating potentials with two tips (Φ_{f2} and Φ_{f3}), separated poloidally by $\delta_p = 8$ mm and a third tip (Φ_{f1}) between them, radially sticking out by $\delta_r = 5$–8 mm.[16] E_r was calculated as $[\Phi_{f1} - (\Phi_{f2} + \Phi_{f3})/2]/\delta_r$ and the Reynolds stress was estimated as $\langle \tilde{v}_r \tilde{v}_p \rangle = \langle \tilde{E}_r \tilde{E}_p \rangle / B^2$, where $E_p = (\Phi_{f2} - \Phi_{f3})/\delta_p$ and the tilde represents fluctuation components, at a frequency over 10 kHz with turbulence dominating the spectrum.[8]

Low-frequency potential and E_r fluctuations, with strong correlation to the oscillations on the divertor Dα signals, have been detected by the probes up to ~1.6 cm inside the separatrix which is roughly half way to the top of the pedestal. The pedestal width in these plasmas is ~3 cm as measured by reflectometry and Thomson scattering. Data beyond 1.6 cm are unavailable, mainly limited by strong second electron emission from the probes. Figure 2 shows the cross-power and cross-phase spectra between floating potentials at two locations toroidally separated by 89° (black solid curve), poloidally separated by 8 mm (blue dotted curve), and radially separated by 8 mm (red dashed curve), respectively, which indicates that the low-frequency fluctuations in the floating potentials at different toroidal, poloidal, and radial locations are strongly correlated with each other, with nearly no phase differences poloidally and toroidally, but with finite phase difference radially, thus providing strong evidence for ZFs.[15]

Furthermore, during the cycle state, the probes detected a high-frequency-broadband (0.05–1 MHz) turbulence in the plasma edge steep-gradient region. Its peak frequency is usually higher than 100 kHz with the frequency band being clearly separated from the fluctuations below 50 kHz, as shown in the time-frequency spectrum of the floating potential at ~1.6 cm inside the separatrix in Fig. 3(b) and ~1 cm inside the separatrix in Fig. 4(b). The L-H transition at 3.8374 s immediately follows a burst of negative spikes in the Reynolds stress [Fig. 3(c)] and potential fluctuations [Fig. 3(b)]. Before the transition, the spectral power of the edge turbulence is mainly below 0.2 MHz, then is strongly suppressed after the transition and replaced by high-frequency turbulence. Significant Reynolds stress and its radial gradient are driven, with magnitude increasing along

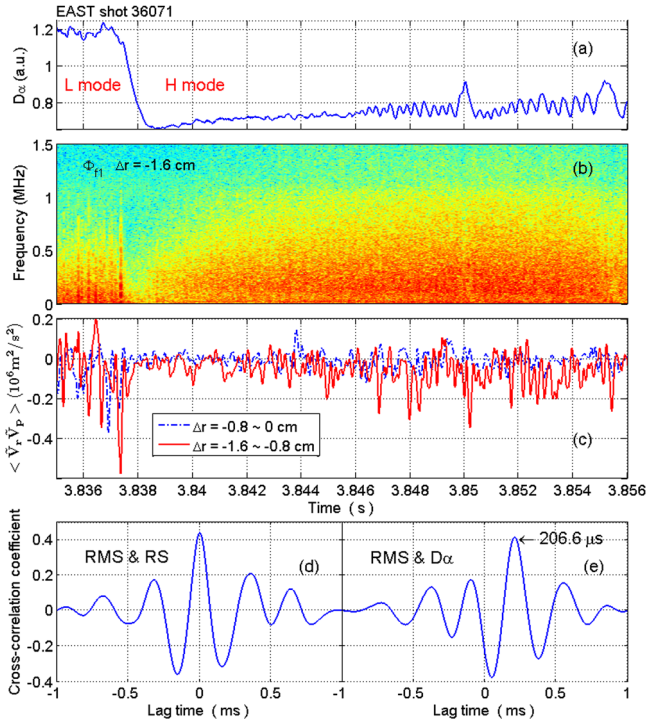

FIG. 3. (a) Dα emission near the inner target of the lower divertor, (b) time-frequency spectrum of a floating potential signal Φ_{f1} at ~1.6 cm inside the separatrix, (c) turbulent Reynolds stress measured by a probe array near the separatrix ($\Delta r = -0.8$–0 cm, blue dashed curve) and another probe array deeper inside the plasma ($\Delta r = -1.6 \sim -0.8$ cm, solid red curve). Cross-correlation coefficient between fluctuation RMS level of Φ_{f1} and (d) radial gradient of the Reynolds stress, (e) Dα emission.

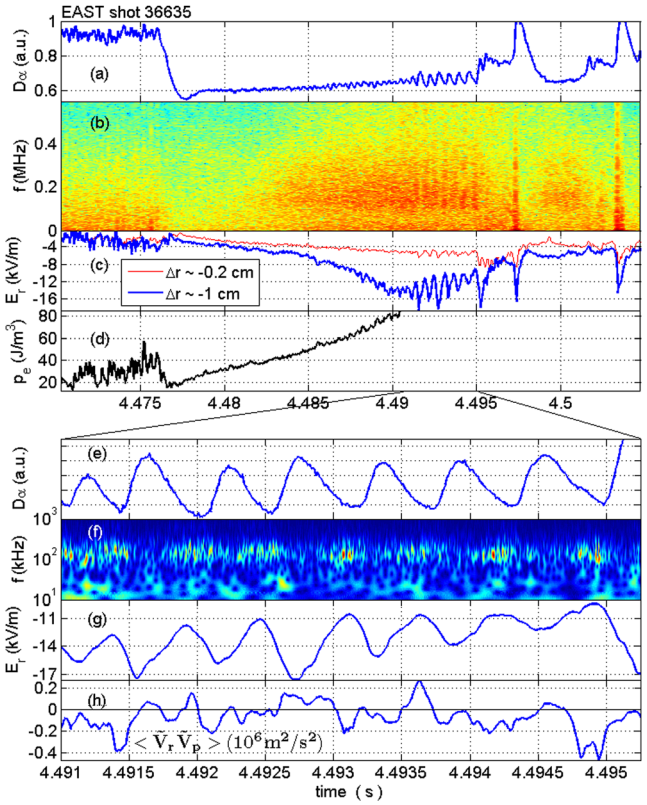

FIG. 4. (a) Dα emission near the inner target of the lower divertor, (b) time-frequency spectrum of a floating potential signal at ~1 cm inside the separatrix, (c) radial electric field measured at ~0.2 cm (thin red curve) and ~1 cm (thick blue curve) inside the separatrix simultaneously, (d) electron pressure measured by a triple-probe array at ~0.2 cm inside the separatrix, (e) zoom of the Dα signal, (f) wavelet time-frequency spectrum of the same floating potential signal as that in (b), (g) radial electric field, and (h) turbulent Reynolds stress measured at ~1 cm inside the separatrix by the probes.

with the intensity of the high-frequency turbulence, as shown in Fig. 3(c). In this case, the Reynolds stress measured near the separatrix ($\Delta r = -0.8$–0 cm) varies around zero while that measured deeper inside the plasma ($\Delta r = -1.6 \sim -0.8$ cm) shows strong negative spikes. The transient radial gradient is up to $\langle \tilde{v}_r \tilde{v}_p \rangle / \delta r \sim 3 \times 10^7 m/s^2$ during the cycle state, where δr is the radial distance between the two probe arrays. As expected, the radial gradient of Reynolds stress is in phase with the turbulent fluctuation RMS level as indicated by the cross-correlation function in Fig. 3(d), since Reynolds stress is driven by turbulent fluctuations. The divertor Dα emission lags the RMS level by 206.6 μs as shown in Fig. 3(e), consistent with the scrape-off layer (SOL) parallel transport time scale, $\tau_{\|} = L_{\|}/C_s \sim 200\,\mu s$, where $L_{\|}$ (~10 m) is the SOL parallel connection length and C_s (~50 km/s) is the sound speed. The peak of cross-correlation coefficient is ~0.4. The weak correlation could be due to high statistical noise in the probe data.

In another shot, the electron temperature, density, and pressure, $p_e = T_e n_e$ [Fig. 4(d)], near the separatrix were measured by a triple-probe array following the standard technique.[14] The E_r in Fig. 4(c) was measured by the probes at ~0.2 cm (thin red curve) and ~1 cm (thick blue curve) inside the separatrix simultaneously. A slow buildup of the negative mean E_r and edge electron pressure can be seen prior to the L-H transition at 4.476 s. Shortly after the transition, the high-frequency turbulence appears and its amplitude grows with time [Fig. 4(b)], accompanying the increase of edge plasma pressure [Fig. 4(d)]. To a simple approximation, turbulence can survive in the H-mode pedestal when the instability linear growth rate or nonlinear decorrelation rate exceeds the local $\mathbf{E} \times \mathbf{B}$ shearing rate. The decorrelation rate of the high-frequency turbulence is calculated as the inverse of the turbulent autocorrelation time, $\tau_c^{-1} \sim 0.3 \times 10^6\,s^{-1}$. It is of the same order of the local $\mathbf{E} \times \mathbf{B}$ shearing rate, $\omega_s \sim \Delta E_r / B \Delta r \sim 0.5 \times 10^6\,s^{-1}$, estimated from the radial gradient of E_r using the probe data as shown in Fig. 4(c). A negative mean E_r and an oscillation in the E_r with amplitude up to 30% of the mean E_r develop simultaneously [Fig. 4(c)]. The time evolution of the mean E_r largely follows that of the edge electron pressure [Fig. 4(d)]. At 4.491 s, the turbulence level begins to saturate while the E_r oscillation amplitude grows to a high value. Finally, the high-frequency turbulence is strongly suppressed at 4.495 s, and at the same time, the oscillations disappear. This clearly indicates that the presence of the oscillations or cycle state is strongly correlated with that of the high-frequency turbulence. The electron pressure data after 4.491 s are unavailable in this shot since an arcing on the probes occurred.

Figures 4(e)–4(h) show the expanded time traces. The E_r at ~1 cm inside the separatrix [Fig. 4(g)] appears to be well correlated with the oscillation on the divertor Dα signal [Fig. 4(e)]. The high-frequency turbulence, as shown in the time-frequency wavelet spectrum in Fig. 4(f), appears to be periodically suppressed by the E_r oscillations. Here, the spectrum was calculated as a continuous wavelet transform of the same floating potential signal as that in Fig. 4(b) using a complex-Gauss wavelet. By carefully tracking the time series, one can see that the high-frequency turbulence is suppressed when the local E_r becomes more negative, i.e., stronger E_r shear. Here, $|E_r|$ lags turbulent fluctuation level by a phase angle between $\pi/2$ and π (anti-correlation). For a predator-prey oscillation with a duty cycle near one, a $\pi/2$ phase lag of the ZF with respect to the turbulence level is expected.[11] However, in the presence of a strong equilibrium flow shear, the phase delay between turbulence level and ZF will shift towards π, as predicted by a theory[11] and demonstrated recently by modeling.[12] The theory proposes that the equilibrium flow shear inhibits the ZF growth due to weakening of the response of wave spectrum to a seed ZF. This shifting towards π has indeed been observed recently in DIII-D experiments during the I-phase as approaching the final H-mode transition.[10] In our case, strong equilibrium flow shear exists in the H-mode pedestal region, which could explain the observed phase deviation from $\pi/2$. It should be pointed out that this physics has not been taken into account in the predator-prey model which will be presented in below, so that a $\sim\pi/2$ phase lag of the ZF amplitude with respect to the turbulence intensity appears in Fig. 5. In principle, the contradiction to the model can be resolved if this physics is included. However, for simplicity, this physics has been omitted in the following model.

The turbulent Reynolds stress [Fig. 4(h)] also predominantly oscillates at the same frequency. The Reynolds stress

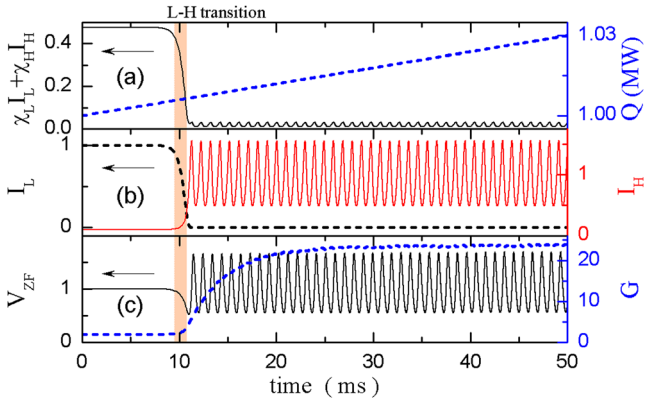

FIG. 5. Time evolution of (a) turbulence-driven transport ($\chi_L I_L + I_H \chi_H$, black solid curve) and power flux (Q, blue dashed curve), (b) intensities of low-frequency turbulence (I_L, black dashed curve) and high-frequency turbulence (I_H, red solid curve), (c) zonal-flow shear (V_{ZF}, black solid curve), and pressure gradient (G, blue dashed curve). The shadow bar at 10 ms indicates the moment of the L-H transition.

statistically increases while the high frequency turbulence is present, although the correlation is weak. The peak cross-correlation coefficient between the E_r and the Dα emission/turbulence envelop/Reynolds stress is 0.80/0.78/0.30, respectively. Here, the Reynolds stress is estimated based on a 0.5-ms time average of local measurements instead of a flux-surface average, which may explain the observed low correlation. The oscillations on the divertor Dα signal [Fig. 4(e)] indicate that this high-frequency turbulence may drive transport and the recycling of neutrals near the divertor target. The latters may therefore be modulated by the ZF-regulated cross-field transport into the SOL. The energy gain by the ZFs in one cycle is estimated to be $0.5 m_i (E_r/B)^2 (1 + 2q_{95}^2) \sim 1 \times 10^{-18}$ J,[1] which is of the same order of the energy loss by the high-frequency turbulence, $e|\Phi| + 0.5 m_i (\tilde{E}_p/B)^2$. Here, $|\Phi|$ is the reduction in potential-fluctuation envelope. The detailed wavelet bicoherence analysis shows a strong three-wave coupling between the high-frequency turbulence and the low-frequency E_r oscillations.

A small amount of stored energy perturbation was induced by the oscillations, $\Delta W/W < 0.1\%$, as estimated using data from Langmuir probes embedded in the divertor targets, divided by the total thermal energy in the plasma. The timescale for induced stored energy loss is ~1 ms which is nearly two order of magnitude shorter than the energy confinement time. As expected, these oscillations do not appear to significantly affect the H-mode confinement, as indicated in Fig. 1(a), where the $H_{98y,2}$ factor is nearly 1. The good confinement can even be achieved with input heating power near the L-H transition threshold. Because of the improved confinement, the plasma density and diamagnetic energy continue to increase in Fig. 1 until this cycle state is replaced by a short ELM-free phase, and then followed by the Type-III ELMs. The presence of the cycle state dramatically delays the occurrence of the first large ELM, see Fig. 1. Such a cycle state has been obtained under a rather wide range of operation conditions: $B_t = 1.4$–2 T, $I_p = 0.4$–0.8 MA, $\bar{n}_e = 2$–6×10^{19} m^{-3}, elongation $\kappa = 1.64$–1.94, lower triangularity $\delta_{low} = 0.44$–0.58, $q_{95} = 2.7$–5.0, collisionality at pedestal top $\nu^*_e = 0.5$–2, double null or single null configuration with favorable and unfavorable ∇B-drift direction.

Another interesting feature of the cycle state is that there is an initial growth phase with a duration of ~10 ms. During this phase, the oscillation frequency decreases typically from ~3 kHz to ~1 kHz, and the amplitude increases with time until finally saturating, as indicated by the divertor Dα signal at 3.257–3.278 s in Fig. 1(b), 3.840–3.856 s in Fig. 3(a), and 4.480–4.495 s in Fig. 4(a). Moreover, the oscillation was observed to be accompanied by small-amplitude ($\tilde{B}/B_t < 1 \times 10^{-5}$) axisymmetric magnetic perturbations (toroidally symmetrical and nearly up-down mirror symmetrical, i.e., m/n = 1/0 in terms of poloidal/toroidal mode number) as detected by Mirnov coil arrays installed in the vacuum chamber. These magnetic perturbations are likely to be caused by a small displacement in the plasma equilibrium due to the loss of stored energy.

III. MODELING

A new phenomenological model has been developed to better understand this cycle state, incorporating the evolution of ZFs, pressure gradient and turbulence in two frequency ranges as a self-consistent zero-dimensional (0D) predator-prey system. This model consists of four coupled equations,

$$\partial_t I_L = \gamma_L Q I_L - \alpha_L V_{ZF} I_L - \nu_L V_{MF} I_L, \quad (1)$$

$$\partial_t I_H = \gamma_H Q I_H - \alpha_H V_{ZF} I_H, \quad (2)$$

$$\partial_t V_{ZF} = \nu_L V_{MF} I_L + \alpha_L V_{ZF} I_L + \alpha_H V_{ZF} I_H - \mu V_{ZF}, \quad (3)$$

$$\partial_t G = \kappa Q - \chi_L I_L G - \chi_H I_H G - \tau^{-1} G. \quad (4)$$

Here, Eqs. (1) and (2) describe the evolution of the low- and high-frequency turbulence intensities, I_L and I_H, respectively, and Eq. (3) describes the evolution of the ZF shear, $V_{ZF} \propto \partial_r \tilde{V}_E$, by extending the previous predator-prey model[4,11] to accommodate one predator and two prey. The evolution of the pressure gradient, G, is described by Eq. (4), where G is enhanced by the power flux, Q, across the plasma boundary, but reduced by the neoclassical transport on the timescale of τ and turbulent transport driven by both low- and high-frequency turbulence, as represented by $\chi_L I_L G$ and $\chi_H I_H G$, with χ_L and χ_H being thermal transport coefficients in Eq. (4). In the model, we simply assume a flux drive for both turbulence components, and so the first terms on the right-hand side of Eqs. (1) and (2) are proportional to Q.

In this model, the kinetic energy is conserved during the energy-exchange processes between turbulence and ZFs. The ZFs draw free energy from both low- and high-frequency turbulences by the shear induced Reynolds stress.[4] The second and third terms on the right-hand side of Eq. (1) represent the shear suppression of low-frequency turbulence by ZF shear and mean $\mathbf{E} \times \mathbf{B}$ flow shear, $V_{MF} \propto \partial_r \langle V_E \rangle$, respectively. Here, we have used the approximation to the ion radial force balance equation, $V_{MF} = G^2$, following the expression in reference.[11] The mean-flow shear is generated by the neoclassical transport mechanisms, thus solely depending on the pressure gradient, G. The high-frequency

turbulence has a much higher decorrelation rate than the low-frequency turbulence, which might imply a smaller spatial scale, since the poloidal size of turbulence eddies is roughly proportional to the decorrelation time, $L_p \sim V_E \tau_c$, by assuming that turbulence propagation is dominated by the $\mathbf{E} \times \mathbf{B}$ drift. Considering disparate spatial scales of the mean-flow shear and the high-frequency turbulence, we assume that the high-frequency turbulence is not sensitive to the mean-flow shear. As a result, a mean-flow-shear term is absent in Eq. (2). Furthermore, the ZFs are subjected to a strong frictional damping as described by the last term in Eq. (3).

This system of equations is solved numerically. To illustrate how the plasma evolves into a cycle state from the L mode (Low-confinement mode), Fig. 5 shows the time evolution of turbulence-driven transport ($\chi_L I_L + I_H \chi_H$), power flux (Q), intensities of low-frequency turbulence (I_L) and high-frequency turbulence (I_H), ZF shear (V_{ZF}), and pressure gradient (G), obtained from the model assuming constant values for the other coefficients. The shadow bar at 10 ms indicates the moment of the L-H transition. The system is driven by Q, which is the source of free energy and the control parameter. It increases from 1 MW at a slow ramping rate of 0.6 MW/s, as shown in Fig. 5(a). Before the L-H transition, significant transport and finite ZFs are driven by the low-frequency turbulence. When approaching the transition, as the power flux increases, the pressure gradient steepens slowly, resulting in an increase in the mean-flow shear, Reynolds stress, and energy transfer into ZFs, thereby suppressing the turbulence level and associated transport. After the transition, the pressure gradient builds up due to improved confinement, thus allowing a further growth of the mean-flow shear, which then sustains a state of suppressed low-frequency turbulence and locks in the H mode. In the absence of a turbulent drive, the ZFs begin to die away. As the ZF shear is reduced, the high-frequency turbulence becomes unstable. It grows up shortly after the transition, transferring energy into the ZFs, thus stopping the decay of the ZFs. However, when the ZFs grow up to a high level the high-frequency turbulence is suppressed. Moreover, as the turbulent drive is reduced, the ZFs start to decay again. This process repeats so that the ZFs and the high-frequency turbulence compete with each other, leading to a predator-prey cycle state, as shown in Fig. 5. A small-amplitude oscillation also appears in the turbulence-driven transport [Fig. 5(a)], as the transport driven by the high-frequency turbulence is modulated by the cycles. The L-H transition and oscillation behavior appear to be similar to those on the divertor Dα signal in Fig. 1(b). The preliminary modeling results successfully reproduced the key features of this cycle state. Further study on the effect of the various model coefficients on the characteristic frequency will be addressed in future publications.

IV. SUMMARY

In summary, a new turbulence-ZFs cycle state has been discovered in the H-mode edge barrier region of magnetically confined toroidal fusion plasmas. Detailed measurements from two toroidally separated fast-moving Langmuir probes demonstrated that oscillatory ZFs exist in the steep-gradient region and a predator-prey interaction between the ZFs and a high-frequency-broadband (0.05–1 MHz) turbulence results in intermittent transport events across the edge transport barrier. The growth, saturation, and disappearance of the ZFs are strongly correlated with those of the high-frequency turbulence, thus strongly suggesting a causal link between them. A new self-consistent 0-D predator-prey model, incorporating the evolution of ZFs, pressure gradient and turbulence at two different frequency ranges, was developed and successfully reproduced the key features of this newly observed cycle state. This demonstrates that turbulence-ZFs interactions also exist in a strong barrier region, well after the formation of a transport barrier, and act to generate this predator-prey cycle state.

ACKNOWLEDGMENTS

This work was supported by the National Magnetic Confinement Fusion Science Program of China under Contracts Nos. 2011GB107001, 2010GB104001, and 2012GB101000, the National Natural Science Foundation of China under Contracts Nos. 11075181, 11021565, 10990212, 10725523, and the Sino Danish Center for Education and Research. We gratefully acknowledge the contribution of the EAST staff.

[1]P. H. Diamond, S.-I. Itoh, K. Itoh, and T. S. Hahm, Plasma Phys. Controlled Fusion **47**, R35 (2005).
[2]F. J. Beron-Vera, M. G. Brown, M. J. Olascoaga, I. I. Rypina, H. Koçak, and I. A. Udovydchenkov, J. Atmos. Sci. **65**, 3316 (2008).
[3]Z. Yan, G. R. McKee, R. J. Groebner, P. B. Snyder, T. H. Osborne, and K. H. Burrell, Phys. Rev. Lett. **107**, 055004 (2011).
[4]P. H. Diamond, Y.-M. Liang, B. A. Carreras, and P. W. Terry, Phys. Rev. Lett. **72**, 2565 (1994).
[5]S. J. Zweben, R. J. Maqueda, R. Hager, K. Hallatschek, S. M. Kaye, T. Munsat, F. M. Poli, A. L. Roquemore, Y. Sechrest, and D. P. Stotler, Phys. Plasmas **17**, 102502 (2010).
[6]T. Estrada, T. Happel, C. Hidalgo, E. Ascasibar, and E. Blanco, Europhys. Lett. **92**, 35001 (2010).
[7]G. D. Conway, C. Angioni, F. Ryter, P. Sauter, J. Vicente, and ASDEX Upgrade Team, Phys. Rev. Lett. **106**, 065001 (2011).
[8]G. S. Xu, B. N. Wan, H. Q. Wang, H. Y. Guo, H. L. Zhao, A. D. Liu, V. Naulin, P. H. Diamond, G. R. Tynan, M. Xu, R. Chen, M. Jiang, P. Liu, N. Yan, W. Zhang, L. Wang, S. C. Liu, and S. Y. Ding, Phys. Rev. Lett. **107**, 125001 (2011).
[9]T. Estrada, C. Hidalgo, T. Happel, and P. H. Diamond, Phys. Rev. Lett. **107**, 245004 (2011).
[10]L. Schmitz, L. Zeng, T. L. Rhodes, J. C. Hillesheim, E. J. Doyle, R. J. Groebner, W. A. Peebles, K. H. Burrell, and G. Wang, Phys. Rev. Lett. **108**, 155002 (2012).
[11]E. J. Kim and P. H. Diamond, Phys. Rev. Lett. **90**, 185006 (2003).
[12]K. Miki, P. H. Diamond, Ö. D. Gürcan, G. R. Tynan, T. Estrada, L. Schmitz, and G. S. Xu, Phys. Plasmas **19**, 092306 (2012).
[13]G. S. Xu, B. N. Wan, J. G. Li, X. Z. Gong, J. S. Hu, J. F. Shan, H. Li, D. K. Mansfield, D. A. Humphreys, and V. Naulin, Nucl. Fusion **51**, 072001 (2011).
[14]W. Zhang, J. F. Chang, B. N. Wan, G. S. Xu, C. J. Xiao, B. Li, C. S. Xu, N. Yan, L. Wang, S. C. Liu, M. Jiang, and P. Liu, Rev. Sci. Instrum. **81**, 113501 (2010).
[15]A. D. Liu, T. Lan, C. X. Yu, H. L. Zhao, L. W. Yan, W. Y. Hong, J. Q. Dong, K. J. Zhao, J. Qian, J. Cheng, X. R. Duan, and Y. Liu, Phys. Rev. Lett. **103**, 095002 (2009).
[16]G. S. Xu, B. N. Wan, M. Song, and J. Li, Phys. Rev. Lett. **91**, 125001 (2003).